The spectrum of radioactive water vapor: the $H_2^{19}O$ radio-isotopologue

Boris A. Voronin[1,2] · Jonathan Tennyson[3] · Tatyana Yu. Chesnokova[2] · Aleksei V. Chentsov[2] · Aleksandr D. Bykov[2]

Abstract

The absorption spectrum of $H_2^{19}O$, a radioactive isotopologue of the water molecule, is predicted using variational nuclear motion calculated based on a high precision potential energy function and ab initio dipole moment surface. Vibrational - rotational energy levels and wave functions, line centers and Einstein coefficients for dipole transitions are calculated. Predicted transition wavenumbers are improved by extrapolating known empirical energy levels of the stable $H_2^{16}O$, $H_2^{17}O$ and $H_2^{18}O$ isotopologues to $H_2^{19}O$. A line list for possible atmospheric application is presented which includes air line broadening coefficients. The calculations span a wide spectral range covering infrared and visible wavelengths, and are appropriate for temperatures up to 1000 K. Windows suitable for observing absorption by $H_2^{19}O$ are identified and comparisons made with the infrared spectra of water vapor in natural abundance, $H_2^{15}O$ and $H_2^{14}O$.

Introduction

Water is one of the most important substances for humanity and its environment. Therefore, there are a large number of scientific works studying water and, in particular, the water molecule, its properties, reactivity, spectra, and isotopic composition.

Measurements and calculations of the absorption, emission, or scattering spectra of radioactive water isotopologues (radio-isotopologues) are of interest for many reasons. Radio-isotopologues of atmospheric gases, including H_2O, are formed in the atmosphere when the Earth is irradiated by cosmic rays. The interaction of atmospheric molecules with cosmic rays leads, for example, to the accumulation in the atmosphere of triterated water, $HT^{16}O$, and the carbon dioxide radio-isotopologue $^{14}CO_2$ [11]. It has been shown that various radio-isotopes of beryllium, carbon, nitrogen, and oxygen can be produced by lightning discharges [3, 29], which also leads to the appearance of radio-isotopologues such as $^{16}O^{15}O$ and $H_2^{15}O$ in the atmosphere. We [51] previously showed that radio-isotopologue $H_2^{15}O$ is apparently present in trace amounts in the atmosphere during thunderstorms. Radioactivity occurring during a thunderstorm front is discussed by Bordonskiy [4].

Oxygen-19 is also found in the cooling circuits of nuclear reactors [8, 55], Nemoto et al. [28] discovered that radio-isotopologues of water are formed when a target containing deuterium is irradiated with femtosecond laser pulses, and the mechanism of production of these isotopologues is similar to their production in lightning discharges. Other radio-isotopologues of water, $H_2^{19}O$ and $H_2^{20}O$, are produced in the primary cooling circuits of nuclear reactors [43]. The contribution of these isotopic modifications to radioactivity fields at nuclear power plants should be taken into account. Inside water-cooled fusion reactors, water is

✉ Jonathan Tennyson
j.tennyson@ucl.ac.uk

Boris A. Voronin
vba@iao.ru

Tatyana Yu. Chesnokova
ches@iao.ru

Aleksei V. Chentsov
cav@iao.ru

Aleksandr D. Bykov
bykov@iao.ru

1 Instituto de Fisica Gleb Wataghin, Universidade Estadual de Campinas, Campinas, SP 13083-859, Brazil

2 V.E. Zuev Institute of Atmospheric Optics SB RAS, sq. Ak. Zuev 1, 643021 Tomsk, Russia

3 Department of Physics and Astronomy, University College London, Gower Street, London WC1E 6BT, UK

irradiated by neutrons when it passes the reactor core. This causes higher doses around the primary coolant: the main observed nuclides are ^{16}N and ^{19}O [19]. Similarly, these radioisotopes are also found in pressurized water reactors (PWRs) [43, 55] which has raised safety concerns [12, 17]. So far, only nuclear spectra (decay of the ^{19}O atom) have been recorded [8]. It is clear that ^{19}O lives long enough to form water molecules; however, the spectrum if $H_2^{19}O$ has yet to be investigated.

In the 1970 abstract review [1] there is mention of work on ^{19}O and $H_2^{19}O$ (Investigation of the recoil chemistry of ^{19}O and of radiolysis of water by reactor radiation. Blaser W. 1970. 79p. Dep. SFSTI (in German)). This abstract discussed the energies of ^{19}O and some molecules such as $H_2^{19}O$, $H^{16}O^{19}OH$, $^{16}O^{19}OH$ and $^{16}O^{19}O$. A number of monographs discussing ^{19}O species, including water, are available [2, 15, 20, 21, 23, 25, 30, 34, 36–39, 44]. In addition, there are a large number of monographs that consider the 6 main isotopes of oxygen from $H_2^{14}O$ to $H_2^{19}O$.

To address the various scientific and technical problems involved with the presence of radioactive water, detailed information is needed on the spectra of water radio-isotopologues. Since measuring the spectra of short-lived radioactive substances is costly and difficult due to both safety issues and the short lifetime of radio-isotope, the most convenient way to determine their spectrum is to calculate it using a high-precision methods benchmarked for the stable isotopologues against the extensive available experimental data. We have previously computed predicted spectra for $H_2^{15}O$ [51, 53] and $H_2^{14}O$ [52]. The present work is aimed at studying the vibrational and rotational states of the short-live radio-isotopologue of the water molecule $H_2^{19}O$, and the associated spectrum at infrared (IR) and visible wavelengths. The calculations are carried out by combining two different techniques. The first of them uses a high-precision potential energy surface [6], which includes non-adiabatic and relativistic corrections, and the variational nuclear-motion code DVR3D [40]. The second step employs a simple quadratic approximation based on using the known empirical energy levels of three stable isotopologues $H_2^{16}O$, $H_2^{17}O$ and $H_2^{18}O$ to improve the predicted transition frequencies. Calculations of vibrational energy levels of $H_2^{19}O$ as well as other isotopologues of water vapor ($H_2^{X}O$, where X =11,...,26) were early presented in Ref. [47].

Table 1 presents data on different oxygen isotopes. It can be seen that after ^{15}O and ^{14}O, ^{19}O has the longest half-life. This also indicates the importance of predicting the spectrum $H_2^{19}O$.

An key focus of our study is to show that at the current level of development of the theory, expensive and complex experiments can be replaced by calculations without loss of accuracy and reliability. Moreover, calculations within the framework of our semi-empirical approach allow not only the calculation of absorption spectra with high accuracy, but also thermodynamic functions such as the temperature-dependent entropy and heat capacity.

Calculated spectrum and of line list of $H_2^{19}O$

The theoretical absorption spectrum of $H_2^{19}O$ is obtained via direct variational calculation of line centers and intensities for states with rotational levels with $J \leq 20$ using a high accuracy potential energy surface (PES) [6], and an *ab initio* dipole moment surface (DMS) [22]. The calculations were carried out as follows. First, the vibrational-rotational (VR) energy levels and associated wavefunctions for $H_2^{19}O$ were computed using the DVR3D variational nuclear-motion package [40]. These calculations followed the same procedure used for other water radio-isotopologues [52, 53], but with mass of the oxygen atom set to 19.003577969 Da. The calculations were carried out on the "amun" cluster (UCL,

Table 1 Atomic mass and half-life for known isotpes of oxygen ^{X}O, X=13,..,23 [27]

Nuclide	Atomic mass and Uncertainty [Da]	Half-life and Uncertainty	Discovery Year
^{13}O	13.024815435 ± 0.000010226	8.58 ms ± 0.05	1963
^{14}O	14.008596706 ± 0.000000027	70.621 s ± 0.011	1949
^{15}O	15.003065636 ± 0.000000526	122.266 s ± 0.043	1934
^{16}O	15.99491461926 ± 0.00000000032	Stable	1919
^{17}O	16.99913175595 ± 0.00000000069	Stable	1925
^{18}O	17.99915961214 ± 0.00000000069	Stable	1929
^{19}O	19.003577969 ± 0.00000283	26.470 s ± 0.006	1936
^{20}O	20.004075357 ± 0.00000095	13.51 s ± 0.05	1959
^{21}O	21.008654948 ± 0.000012882	3.42 s ± 0.10	1968
^{22}O	22.009965744 ± 0.000061107	2.25 s ± 0.09	1969
^{23}O	23.015696686 ± 0.000130663	97 ms ± 8	1970

London, UK). This procedure has been used to produce a number of line list for H_2O and it isotopologues including BT2, VTT [49], POKAZATEL [33], Conway [10], Hot-Wat78 [32] and VoTe [50].

The line list for $H_2^{19}O$, which we call VoTe-19, is designed for use at room temperature over a wide range of wavenumbers. It contains 72 920 states and 106 680 822 (more then one hundred million) transitions in total. The $H_2^{19}O$ (VoTe-19) line list is available from the ExoMol database www.exomol.com using ExoMol format [41]. Extracts from the States .states and Transition .trans files are shown in Tables 2 and 3, respectively. The $H_2^{19}O$ .trans files contain Einstein A coefficients (in s^{-1}) together with the upper and lower state ID numbers. The transitions are divided into twelve Transition files according the the following spectroscopic ranges: 0–500, 500–1000, 1000–1500, 1500–2000, 2000–2500, 2500–3500, 3500–4500, 4500–5500, 5500–7000, 7000–9000, 9000–14,000, 14,000–25,000 cm^{-1}.

The State file contains a list of ro-vibrational states of $H_2^{19}O$ with the state ID numbers, energy term values (in cm^{-1}), uncertainties (in cm^{-1}) and quantum numbers: the provision of which are discussed below. The exact quantum numbers are the total angular momentum J and the total symmetry $\Gamma = A_1, A_2, B_1, B_2$ in the Molecular Symmetry group $C_{2v}(M)$. The total state degeneracy, g_i is given by $(2J+1)$ times the nuclear spin factor, g_{ns}. ^{19}O has a nuclear

spin of $I = \frac{5}{2}$ which for $H_2^{19}O$ leads to $g_{ns} = 6, 6, 18,$ and 18 for $\Gamma = A_1, A_2, B_1, B_2$, respectively.

In addition, for some of the levels, approximate quantum numbers are given using standard harmonic oscillator - rigid rotor designations: v_1, v_2, v_3, K_a, K_c; the provision of these is discussed below. Here v_1, v_2, v_3 are the normal mode vibrational quantum numbers, K_a and K_c are the oblate and

Table 3 Extract from a .trans file of the $H_2^{19}O$ line list

f	i	A_{fi}
53397	54633	0.32305E−23
25152	24212	0.80174E−20
4853	7956	0.24636E−22
64698	61306	0.62528E−22
38048	36839	0.38686E−19
56019	57261	0.80929E−19
19875	20924	0.13715E−18
54551	48696	0.40687E−24
24031	24993	0.62368E−18
29261	28107	0.12623E−17
26198	27331	0.24941E−17

f: Upper state counting number;

i: Lower state counting number;

A_{fi}: Einstein-A coefficient (in s^{-1})

Table 2 Extract from the .states file of the $H_2^{19}O$ line list

i	$\tilde{E}/cm^{-1}$	g	J	δ/cm^{-1}	v_1	v_2	v_3	K_a	K_c	e/o	Γ_{tot}	$\tilde{E}_D/cm^{-1}$	Code
1	0.000000	6	0	0.000001	0	0	0	0	0	e	A1	0.000000	IE
2	1585.510477	6	0	0.045301	0	1	0	0	0	e	A1	1585.527013	IE
3	3133.674946	6	0	0.089534	0	2	0	0	0	e	A1	3133.680018	IE
4	3646.583546	6	0	0.104187	1	0	0	0	0	e	A1	3646.545140	IE
5	4640.650684	6	0	0.132590	0	3	0	0	0	e	A1	4640.650684	Ca
6	5215.434906	6	0	0.149012	1	1	0	0	0	e	A1	5215.425140	IE
7	6100.343362	6	0	0.174296	0	4	0	0	0	e	A1	6100.349223	IE
8	6747.186711	6	0	0.192776	1	2	0	0	0	e	A1	6747.174726	IE
9	7179.236738	6	0	0.205121	2	0	0	0	0	e	A1	7179.234201	IE
10	7407.596097	6	0	0.211645	0	0	2	0	0	e	A1	7407.572789	IE

i: state identifier;

$\tilde{E}$: state term value, DVR3D or pseudo-experimental;

g: state degeneracy;

J: state rotational quantum number;

δ: energy uncertainty;

$v_1 - v_3$: normal mode vibrational quantum numbers;

K_a and K_c: state oblate and prolate quantum numbers;

e/o even or odd - K_c: state oblate and prolate quantum numbers;

Γ_{tot}: total symmetry in $C_{2v}(M)$;

$\tilde{E}_D$: state term value, DVR3D;

Code - Ca (Calculated by DVR3D) or IE - Isotopologue Extrapolation (Pseudo-experimental)

prolate rotational quantum numbers (projection of the angular momentum on the *a* and *c* molecular axes, respectively).

DVR3D only supplies rigorous quantum numbers which for H_2O correspond to *J*, parity and whether the state is ortho or para. To provide the approximate rotation and vibration quantum labels, namely v_1, v_2, v_3, K_a and K_c, we matched the $H_2^{14}O$ energies to the assigned states of the parent isotopologue $H_2^{16}O$ as provided in the VoTe line list [50], which was based on the calculations with the same PES [50]. Following VoTe, here we also provide the parity of the K_c quantum number, which can be reconstructed from the (rigorous) values of *J* and the total symmetry Γ as shown in [7]. ExoMol [41, 42] standard notation is adopted and the value "NaN" is to denote undetermined quantum numbers.

As an attempt to improve the energy levels, and hence transition wavenumbers, predicted for $H_2^{19}O$, we apply pseudo-experimental corrections given by Eq. (1) below to the set of 3426 empirical energy levels identified as common to all three stable isotopologues of interest. These states are indicated with the label "IE" (isotopologue extrapolation [24]) in contrast to all other, calculated values, labelled with "Ca". Following the pseudo-experimental extrapolation method proposed in [32, 33], we use the obs.-calc. residuals obtained for the parent isotopolgue to obtain empirical corrections to the ro-vibrational energy values of the minor isotopologues of water as follows:

$$E_N^{corr} = E_N^{calc} + E_{16}^{obs} - E_{16}^{calc}, \tag{1}$$

where E_N^{calc} is a DVR3D energy calculated for a isotopologue, $N = 17, 18, 19$, and $E_{16}^{obs} - E_{16}^{calc}$ is an empirical correction estimated as the difference between the calculated and experimental energies of $H_2^{16}O$. The approach is based on the assumption that the main source of the error is from the inaccuracy of the Born-Oppenheimer PES of water, which should affect all four isotopologues similarly and was shown to work well for $H_2^{18}O$ and $H_2^{17}O$ [32, 33].

The provision of uncertainties in the energy levels is now a formal part of the ExoMol data structure [41, 42]. For the pseudo-experimental values, the uncertainties are estimated as the the obs.-calc. residuals of the $H_2^{17}O$ isotopologue obtained as the difference between the W2020 and DVR3D energy values. For the other levels, formula (2) was used:

$$unc = \Delta\xi\tilde{E} + \Delta BJ(J + 1), \tag{2}$$

with $\Delta\xi$=1/35000 cm^{-1} and ΔB=0.0005 cm^{-1}. Formula (2) was obtained via correlation and auto-correlation methods [5] applied to the W2020 [14] data of the three isotopologues in conjunction with the method of Voronin et al. [52]. For $H_2^{16}O$, we can use residuee for the 19225 empirical energy levels provided W2020, and calculate the errors using formula (2). For rotational-vibrational states, where the energies of all three $H_2^{16}O$ isotopologues were present

in W2020, we used the double uncertainty of the main isotopologues, since it is very small.

A total 3426 levels were replaced by the pseudo-experimental values. The maximum deviations of these changes do not exceed 0.1 cm^{-1}.

Spectrum of $H_2^{19}O$ for applications

The line list produced was used to model spectra of $H_2^{19}O$.

A 296 K, room temperature $H_2^{19}O$ line list was generated using the intensity threshold of >10^{-30} cm/molecule for atmospheric applications containing 250 224 lines. The line list is provided as part of the supplementary material in a HITRAN-like format [16], see Table 4.

The HITRAN database provides data for seven isotopologues of water using the following isotopologue codes: 11($H_2^{16}O$), 12($H_2^{18}O$), 13($H_2^{17}O$), 14(HD^{16}O), 15(HD^{18}O), 16(HD^{17}O), 17(D$_2^{16}$O). We adopted 18 as a code for $H_2^{15}O$ [53] and 10 for $H_2^{14}O$ [52]; here we use 19 for $H_2^{19}O$. None of this number have yet to be adopted by HITRAN. The line list consists of the isotopologue code (19) (Molecule number 1 + Isotopologue number 9), line positions, 296 K intensities (cm/molecule), Einstein coefficients (s^{-1}), air-broadened widths (γ_{air}, cm^{-1}/atm), self-broadened widths (γ_{self}, cm^{-1}/atm), temperature dependence component of air n_{air}, line shifts (set to 0.0 cm^{-1}) and ro-vibrational quantum number. The line broadening parameters were evaluated using the *J* and '*JJ*−dependency' methods [46, 48]. For the temperature-dependence exponent n_{air} (unitless) we assumed the water vapor air-broadened half-widths from Table 7 of HITRAN2004 [35].

Partition function, *Q*(*T*), for $H_2^{19}O$ as a function of temperature, *T*(K).

Using vibrational-rotational energy levels, the partition function of $H_2^{19}O$ was calculated for different temperatures up to 1000 K using

$$Q(T) = \sum_i g_i \exp\left(-\frac{E_i}{kT}\right). \tag{3}$$

Fig. 1 shows a comparison of partition functions *Q*(*T*) of the $H_2^{19}O$, $H_2^{16}O$ and $H_2^{15}O$ species for the temperature range from 1 to 1000 K. The main difference is the nuclear spin factor, which is 6 times larger for $H_2^{19}O$ than for $H_2^{16}O$. Furthermore, the partition function of $H_2^{16}O$ is significantly more complete, with the levels from [50] covering the rotational excitations up to *J* = 50.

In principle, with a set of levels up to 25,000 cm^{-1} and up to *J* = 20, our partition function of $H_2^{19}O$ should be

Table 4 Examples spectrum of $H_2^{19}O$ for applications

C	$\tilde{\omega}$	Intensity	A.coeff	γ_{air}	γ_{self}	E''	k_T	shift	$v_1' v_2' v_3'$	$J' K_a' K_c'$	$v_1'' v_2'' v_3''$	$J'' K_a'' K_c''$
19	0.049770	0.179E−26	0.643E−12	0.0808	0.495	444.534074	0.64	0.0	0 0 0	5 2 3	0 0 0	6 1 6
19	0.100849	0.393E−29	0.107E−10	0.0808	0.495	1911.474732	0.73	0.0	0 1 0	5 1 5	0 1 0	4 2 2
19	0.109513	0.193E−29	0.151E−10	0.0808	0.495	2111.656650	0.73	0.0	0 1 0	5 3 3	0 1 0	4 4 0
19	1.535666	0.138E−28	0.197E−07	0.0284	0.207	3063.921281	0.36	0.0	NaN NaN NaN	14 NaN NaN	0 0 0	15 3 12
19	1.612058	0.103E−29	0.187E−07	0.0537	0.309	3490.471234	0.53	0.0	0 1 0	9 7 2	0 1 0	8 8 1
19	2.167510	0.142E−29	0.272E−06	0.0808	0.495	3574.837000	0.73	0.0	0 2 0	5 2 4	0 2 0	4 3 1
19	2.662134	0.110E−25	0.296E−06	0.0870	0.523	1893.370213	0.77	0.0	0 1 0	4 2 3	0 1 0	3 3 0
19	2.695240	0.275E−27	0.197E−06	0.0808	0.495	2380.912733	0.64	0.0	0 1 0	5 5 1	0 1 0	6 4 2
19	2.819662	0.725E−26	0.504E−06	0.0989	0.478	1729.193474	0.77	0.0	0 1 0	2 2 0	0 1 0	3 1 3
19	3.023634	0.221E−25	0.447E−06	0.0870	0.523	1807.870770	0.77	0.0	0 1 0	4 1 4	0 1 0	3 2 1
19	3.075450	0.109E−27	0.202E−06	0.0537	0.309	2887.401244	0.45	0.0	0 1 0	9 3 6	0 1 0	10 2 9
19	3.321044	0.118E−28	0.221E−06	0.0677	0.372	3072.715103	0.53	0.0	0 1 0	7 7 1	0 1 0	8 6 2
19	3.343575	0.359E−28	0.226E−06	0.0677	0.372	3072.692605	0.53	0.0	0 1 0	7 7 0	0 1 0	8 6 3
19	3.581622	0.146E−26	0.462E−06	0.0808	0.495	2380.028898	0.64	0.0	0 1 0	5 5 0	0 1 0	6 4 3
19	3.707662	0.120E−27	0.259E−06	0.0324	0.224	2725.588226	0.36	0.0	NaN NaN NaN	13 NaN NaN	0 0 0	14 3 11
19	4.391607	0.707E−29	0.457E−06	0.0232	0.198	3418.617109	0.38	0.0	0 0 0	15 6 10	0 0 0	16 3 13

C. molecule num.=1 +isotopologue number=9(19)

$\tilde{\omega}$ Transition wavenumber, cm^{-1};

Intensity at 100% abundance, cm/molecule;

Einstein A-coefficient, s^{-1};

γ_{air} Air-broadened width, cm^{-1}/atm;

γ_{self} Self- broadened width, cm^{-1}/atm;

E'' lower-state Energy, cm^{-1};

k_T Temperature dependence (of air width), dimensionless;

Pressure shift, always zero in our case;

Upper vibrational quanta, v_1', v_2', v_3';

Upper local quanta, J', K_a', K_c';

Lower vibrational quanta, v_1'', v_2'', v_3'';

Lower local quanta, J'', K_a'', K_c''
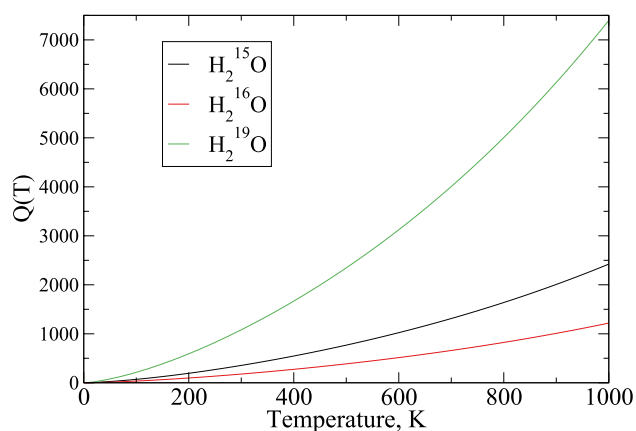
Fig. 1 Partition function $Q(T)$ for $H_2^{19}O$, $H_2^{16}O$ and $H_2^{15}O$ water for temperature range from 1 to 1000 K

appropriate for up to 800 K. Using our results for temperatures higher than this will lead to resulting spectra becoming increasingly incomplete, for more details about partition function see [18, 45]. Our partition function for $H_2^{19}O$ as in presented as a table in the Supplementary materials (Part-Fun-H219O-J20.dat).

Estimated possibility of detecting $H_2^{19}O$ in laboratory conditions

The isotopologues of H_2O have characteristic absorption fingerprints in the IR spectral region and can be analyzed quantitatively and qualitatively using spectroscopic methods. The advantage of high resolution spectroscopy is that it is a non-destructive and non-invasive method which allows simultaneous monitoring of several species in real time.

To reveal spectral windows in which $H_2^{19}O$ could be detected under laboratory conditions, we simulated the

transmission of main isotopologues of H_2O ($H_2^{16}O$, $H_2^{18}O$, $H_2^{17}O$, $HD^{16}O$, $HD^{18}O$, $HD^{17}O$) in natural abundance with the addition $H_2^{19}O$ at high spectral resolution for $T = 294$ K, atmospheric pressure of 1013 mbar, partial pressure of H_2O 18,800 ppm and path length of 100 m. The $H_2^{19}O/H_2O$ ratio was varied from 0.1 to 1%. Transmission was calculated using a line-by-line method [26] with a boxcar apparatus function.

The absorption line parameters, needed for the line-by-line transmission calculation, are the line intensity, S (cm^{-1}/molecule cm^{-2}), position of the line centre, v^* (cm^{-1}), lower-state energy, E (cm^{-1}), air- and self-broadened half-widths γ_{air} and γ_S (cm/atm), and temperature-dependence exponent for γ_{air} - n_{air}. The H_2O absorption lines parameters of main isotopologues were taken from the HITRAN2020 spectroscopic database [16]; our calculated absorption line parameters were used to simulate the transmission by $H_2^{19}O$. Laboratory spectrometers measure the intensity (radiance) of source I, attenuated by gaseous medium at the path length L with the transmission function T and apparatus function f with the spectral resolution Δv. The intensity at wavenumber v is determined by

$$
\begin{aligned}
I(v) &= \int_{\Delta v} I_0(v')T(v')f(v' - v)dv' \\
&= \int_{\Delta v} I_0(v')\exp(-K(v')L)f(v' - v)dv'.
\end{aligned}
\tag{4}
$$

The absorption coefficient, $K(v)$, includes the contributions of all spectral lines in the spectral interval considered and depends on pressure, p, and temperature, t:

$$
K(v,p,t) = \Sigma_{j=1}^M \Sigma_{i=1}^N S_{ij}(t)g(v_{ij}^*, v, p, t)n_j,
\tag{5}
$$

where n_j is the concentration of the jth gas (isotopologue); M is the number of gases (isotopologues); N is the number of spectral lines belonging to the jth gas; and $g(v_{ij}^*, v, p, t)$ is the absorption line profile function. A Voigt line profile [13, 31] is usually empolyed for atmospheric conditions. Line profiles were calculated using broadening line parameters γ and the air temperature-dependence exponent, n_{air}. Transmission spectra of H_2O and $H_2^{19}O$ with a $H_2^{19}O/H_2O$ ratio of 0.5%, calculated with spectral resolution of 0.02 cm^{-1} and 5 cm^{-1} in the 0–15,000 cm^{-1} spectral region, are shown in Fig. 2. It was found that use high spectral resolution of about 0.02 cm^{-1} allows the $H_2^{19}O$ lines to be revealed against of the background H_2O lines at this $H_2^{19}O/H_2O$ concentration ratio.

Transmission spectra of H_2O and $H_2^{19}O$ with $H_2^{19}O/H_2O$ ratio of 0.5% are shown in Fig. 2.

By varying the $H_2^{19}O/H_2O$ ratio, spectral windows suitable for $H_2^{19}O$ detection under laboratory conditions were identified in regions from far to near IR. Examples of the
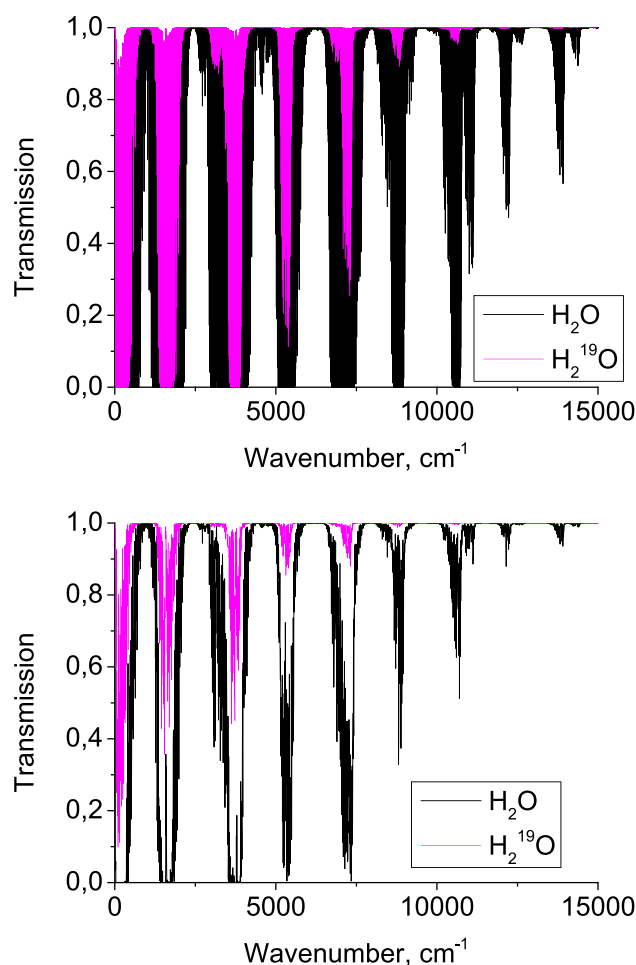

Fig. 2 Transmission spectra of H_2O and $H_2^{19}O$, simulated with spectral resolution of (upper panel) 0.02 cm^{-1} and (lower panel) 5 cm^{-1}; the $H_2^{19}O/H_2O$ ratio is 0.5%

windows are presented in Fig. 3, where one can observe a distinct contribution of the $H_2^{19}O$ lines against a background of H_2O absorption. The spectral lines for perspective $H_2^{19}O$ detection are located in the 411–414, 497–499, 1380–1383, 1902–1905, 1950–1954 and 7109–7112 cm^{-1} wavenumber regions.

In our previous studies [52, 53] the spectra of $H_2^{15}O$ and $H_2^{14}O$ radio-isotopologues were investigated, and the spectral windows, suitable for $H_2^{14}O$ and $H_2^{15}O$ detection, were identified. It is interesting to compare these results with ones obtained for $H_2^{19}O$. This comparison reveals overlapping absorption lines of the radio-isotopologues and allows one to estimate how their interference might impact detections. The transmission spectra of $H_2^{15}O$ and $H_2^{14}O$ with the concentrations of 0.5% relative to H_2O content are shown in Fig. 4 in the spectral windows where the $H_2^{19}O$ can be detected.

As can see in Fig. 4, the $H_2^{19}O$ absorption lines overlap with $H_2^{15}O$ lines in the window of 1380–1383 cm^{-1}, that interfere with the $H_2^{19}O$ detection in this spectral range.

Fig. 3 Spectral windows for the detection of $H_2^{19}O$ at different relative concentration of $H_2^{19}O$. The $H_2^{19}O/H_2O$ ratio varies from 0.1 to 1%
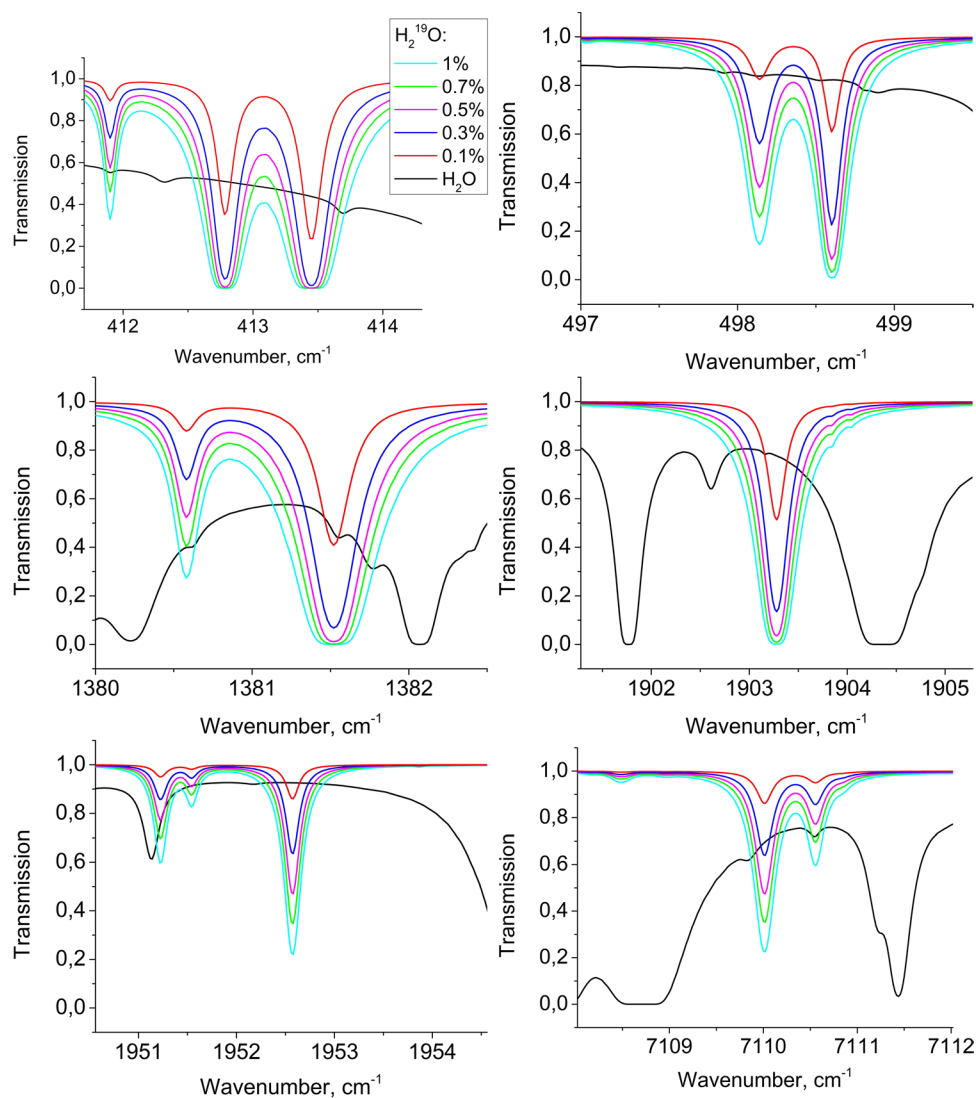
Moreover, the $H_2^{14}O$ lines can influence on the $H_2^{19}O$ measurement in the 7109–7112 cm^{-1} window. According to the transmissions comparisons, the most suitable spectral ranges for detecting $H_2^{19}O$ in laboratory conditions are 412–414 cm^{-1} and 497–499 cm^{-1}.

Conclusion

The first comprehensive calculation of vibrational-rotational spectrum of the water isotopologue $H_2^{19}O$ up to 25,000 cm^{-1} is presented. An empirical line list for the $H_2^{19}O$ is created in the ExoMol-style using calculations based on a high-precision intramolecular potential energy surface which includes allowance for relativistic and non-adiabitic corrections, and *ab initio* dipole moment surfaces. The line list is computed using a spectroscopic model optimised for $H_2^{16}O$ and covers

all transitions up to $J=20$, which means it should be valid for temperatures up to 800 K. The quality of the line list was improved through isotopologue extrapolation of the experimentally-determined energies of $H_2^{16}O$, $H_2^{17}O$ and $H_2^{18}O$. We hope that these theoretical prediction of $H_2^{19}O$ spectra will lead to experimental measurements.

Transmission spectra of $H_2^{19}O$ were simulated varying their concentration. A comparison of the simulated spectra of $H_2^{19}O$ with the transmission spectra of water vapor in natural abundance ($H_2^{16}O$, $H_2^{18}O$, $H_2^{17}O$, $HD^{16}O$, $HD^{18}O$, $HD^{17}O$), and $H_2^{14}O$ $H_2^{15}O$ radio-isotopologues was carried out to find the spectral ranges are best suited for $H_2^{19}O$ detection in laboratory conditions. It was revealed that the spectral windows relevant for the $H_2^{19}O$ detection are placed in the regions of 411–414 cm^{-1}, 497–499 cm^{-1}, 1380–1383 cm^{-1}, 1902–1905 cm^{-1}, 1950–1954 cm^{-1}, and 7109–7112 cm^{-1}, with the two far infrared windows showing the least interference with the other

Fig. 4 Transmission spectra of H_2O in natural abundance and radio-isotopogues: $H_2^{14}O$, $H_2^{15}O$ and $H_2^{19}O$ at concentrations of 0.5% of H_2O
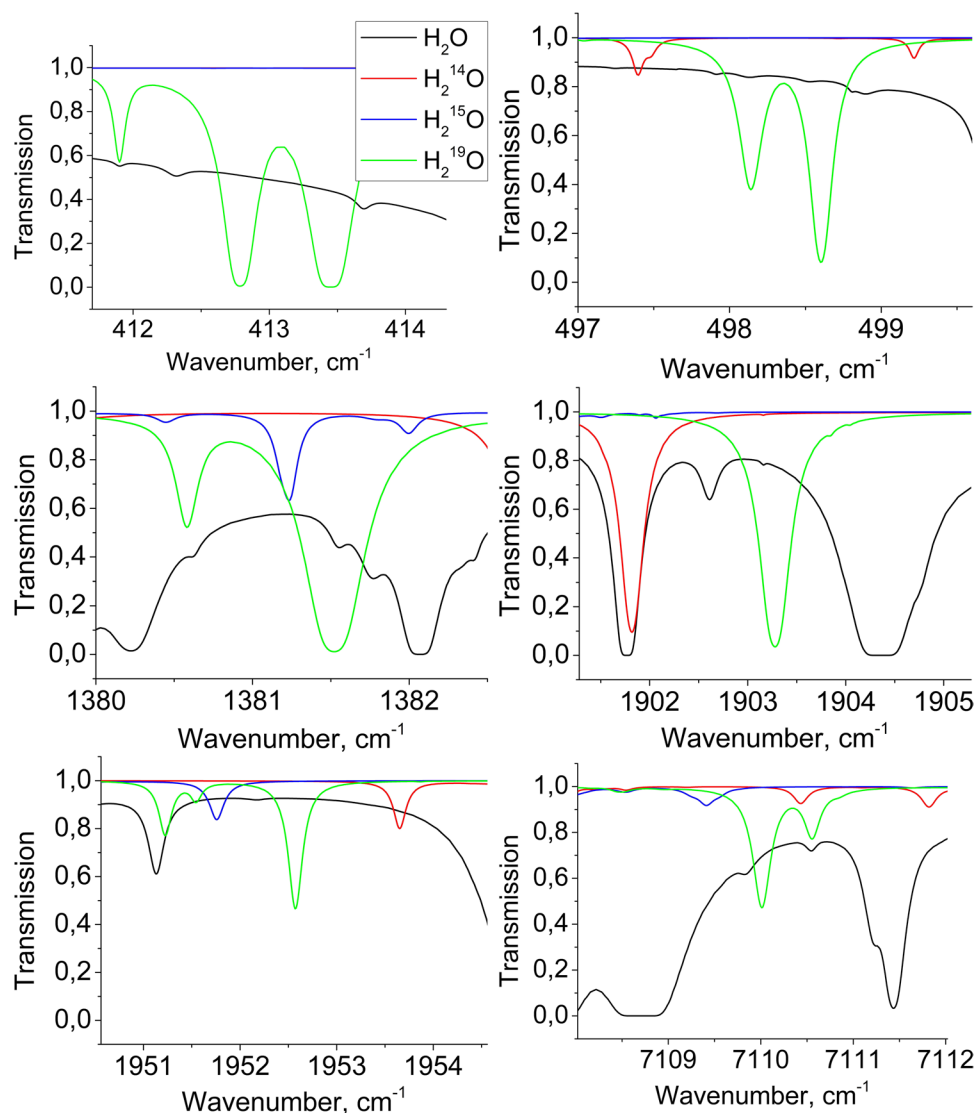
radio-isotopologues. As ^{19}O decays, the concentration of the $H_2^{19}O$ isotopologue will diminish, and its absorption will also decrease. The rate of decrease in absorption at a given wavelength, observed in real time, will provide additional evidence that it the absorptions are due to $H_2^{19}O$.

Our predicted spectrum of $H_2^{19}O$ can be a useful tool for for astrophysics, plasma chemistry, nuclear reactor safety, medical procedures and aid the detection of this radio-isotopologue. It can be expect that $H_2^{19}O$ water plays a greater role in fast-paced complex chemical and nuclear processes than previously assumed. For example, it is possible that short-lived water vapor radio-isotopologues may be responsible for part of the anomalous radiation that is sometimes recorded during thunderstorms [9].

Vibrational-rotational spectroscopy is an effective, nondestructive tool for studying the properties of pollutants and radioactive substances in real time mode. Such studies can help to understand the physicochemical processes involved and to improve the safety of nuclear reactors.

Author Contributions Boris A. Voronin: Term, Validation, Investigation, Writing - Original Draft; Jonathan Tennyson: Supervision, Conceptualization, Resources, Writing - Review & Editing, Methodology; Tatyana Yu. Chesnokova: Investigation, Data Curation, Writing - Review & Editing; Aleksei V. Chentsov: Formal analysis, Visualization; Aleksandr D. Bykov: Conceptualization, Validation.

Data Availibility File `partition-function-H219O.dat` containing only 2 columns, can be found in the supplementary materials. In the first column, the temperature in K, from 1 to 1000 K, in the second column, the value of the partition function at that temperature. File H219O-spectra-296K-E30.dat, see Table (4), can be found in the supplementary materials. At https://ftp.iao.ru/pub/VTT/H219O/ there are

15 files: 12 files containing transitions divided into ranges (format is described in the table 3); one file with the energy levels and identification; one file for atmospheric applications in a format like HITRAN-04 database and one file as an archive for easy download. The full dataset is given as part of the ExoMol database at www.exomol.com. Spectra can be generated using program ExoCross [54].

Declarations

Conflict of interest The authors declare no conflict of interest.

Open Access This article is licensed under a Creative Commons Attribution 4.0 International License, which permits use, sharing, adaptation, distribution and reproduction in any medium or format, as long as you give appropriate credit to the original author(s) and the source, provide a link to the Creative Commons licence, and indicate if changes were made. The images or other third party material in this article are included in the article's Creative Commons licence, unless indicated otherwise in a credit line to the material. If material is not included in the article's Creative Commons licence and your intended use is not permitted by statutory regulation or exceeds the permitted use, you will need to obtain permission directly from the copyright holder. To view a copy of this licence, visit http://creativecommons.org/licenses/by/4.0/.

References

1. Nuclear Science Abstracts (1970) United State Atomic Energy Commission and United States. Energy Research and Development Administration. 24, Oak Ridge Directed Operations, Technical Information Division, https://books.google.com.br/books?id=7Q06AQAAMAAJ
2. Aelion C, Höhener P, Hunkeler D et al (2009) Environmental Isotopes in Biodegradation and Bioremediation. CRC Press
3. Babich LP (2019) Thunderous neutrons. Phys Usp 62:976–999. https://doi.org/10.3367/UFNe.2018.12.038501
4. Bordonskiy GS (2020) Possible mechanisms of anomalous electromagnetic radiation in the earth's atmosphere. Izvestiya, Atmospheric and Oceanic Physics 56:1687–1694. https://doi.org/10.1134/S0030400X11020032
5. Box G, Jenkins G, Reinsel G (2013) Time series analysis: forecasting and control. Wiley series in probability and statistics. Wiley
6. Bubukina II, Polyansky OL, Zobov NF et al (2011) Optimized semiempirical potential energy surface for $H_2^{16}O$ up to 26000 cm^{-1}. Opt Spectrosc 110:160–166. https://doi.org/10.1134/S0030400X11020032
7. Bunker PR, Jensen P (1998) Molecular symmetry and spectroscopy, 2nd edn. NRC Research Press, Ottawa. https://doi.org/10.1142/p371
8. Chung C, Chan CC (1995) Distribution of ^{16}N and ^{19}O in the reactor pool water of the THOR facility. Nuclear Technology 110:106–114. https://doi.org/10.13182/NT95-A35100
9. collaboration TPA, (2011) The pierre auger observatory scaler mode for the study of solar activity modulation of galactic cosmic rays. J Instrument 6:P01003. https://doi.org/10.1088/1748-0221/6/01/P01003
10. Conway EK, Gordon IE, Kyuberis AA et al (2020) Accurate line lists for $H_2^{16}O$, $H_2^{18}O$ and $H_2^{17}O$ with extensive comparisons to theoretical and experimental sources including the HITRAN2016 database. J Quant Spectrosc Radiat Transf 241:106711. https://doi.org/10.1016/j.jqsrt.2019.106711
11. David JC, Leya I (2019) Spallation, cosmic rays, meteorites, and planetology. Progress in Particle and Nuclear Physics 109:103711. https://doi.org/10.1016/j.ppnp.2019.103711
12. Ding S, Xu K, Huang X et al (2006) A $^{16}N/^{19}O$ monitor for leak detection in a steam generator. Nuclear technology 155(3):350–357. https://doi.org/10.13182/NT06-A3767
13. Drayson SR (1976) Rapid computation of the Voigt profile. J Quant Spectrosc Radiat Transf 16(7):611–614. https://doi.org/10.1016/0022-4073(76)90029-7
14. Furtenbacher T, Tóbiás R, Tennyson J et al (2020) W2020: A Database of Validated Rovibrational Experimental Transitions and Empirical Energy Levels of $H_2^{16}O$. J Phys Chem Ref Data 49:033101. https://doi.org/10.1063/5.0008253
15. Gat J (2010) Isotope hydrology: a study of the water cycle. series on environmental science and management. World Scientific Publishing Company
16. Gordon IE, Rothman LS, Hargreaves RJ et al (2022) The HITRAN2020 molecular spectroscopic database. J Quant Spectrosc Radiat Transf 277:107949. https://doi.org/10.1016/j.jqsrt.2021.107949
17. Gupta A, Prasad S, Prabhu S et al (2020) Laser based technique for monitoring heavy water leaks in nuclear reactors: performance validation with conventional techniques. Journal of Instrumentation 15:P03018. https://doi.org/10.1088/1748-0221/15/03/P03018
18. Harris GJ, Viti S, Mussa HY et al (1998) Calculated high temperature partition function and related thermodynamic data for $H_2^{16}O$. J Chem Phys 109:7197–7204. https://doi.org/10.1063/1.477400
19. IAEA (1977) Profile summaries. https://www-pub.iaea.org/MTCD/Publications/PDF/nnMaterials/P1728/Summary_web.pdf
20. Karataglidis S, Amos K, Fraser P et al (2019) A new development at the intersection of nuclear structure and reaction theory. Springer
21. Khublaryan M (2009) Types and Properties of Water, vol 2. EOLSS Publications
22. Lodi L, Tennyson J, Polyansky OL (2011) A global, high accuracy ab initio dipole moment surface for the electronic ground state of the water molecule. J Chem Phys 135:034113. https://doi.org/10.1063/1.3604934
23. Masterson R (2017) Nuclear engineering fundamentals: a practical perspective. CRC Press
24. McKemmish LK, Bowesman CA, Kefala K et al (2024) A hybrid approach to generating diatomic line lists for high resolution studies of exoplanets and other hot astronomical objects: Updates to ExoMol MgO. VO and TiO line lists, RAS Tech Instr (Submitted)
25. Millero F (2016) Chemical Oceanography. CRC Press
26. Mitsel AA, Ptashnik IV, Firsov KM et al (1995) Efficient technique for line-by-line calculating the transmittance of the absorbing atmosphere. Atmos Oceanic Optics 8:847–850
27. National Center for Biotechnology Information (2023) PubChem Element Summary for AtomicNumber 8, Oxygen. https://pubchem.ncbi.nlm.nih.gov/element/Oxygen, accessed 7 May, (2024)
28. Nemoto K, Maksimchuk A, Banerjee S et al (2001) Laser-triggered ion acceleration and table top isotope production. Applied Physics Letters 78(5):595–597. https://doi.org/10.1063/1.1343845
29. Ortega PG (2020) Isotope production in thunderstorms. Journal of Atmospheric and Solar-Terrestrial Physics. 208:105349. https://doi.org/10.1016/j.jastp.2020.105349
30. Penionzhkevich Y, Cherepanov E, Kamanin D, et al (2014) Exotic Nuclei (Iasen-2013) - Proceedings Of The First International African Symposium On Exotic Nuclei. Intelligent Information Systems, World Scientific Publishing Company, https://books.google.com.br/books?id=XyK3CgAAQBAJ
31. Pierluissi JH, Vanderwood PC, Gomez RB (1977) Fast calculational algorithm for the Voigt profile. J Quant Spectrosc Radiat Transf 18(5):555–558. https://doi.org/10.1016/0022-4073(77)90056-5

32. Polyansky OL, Kyuberis AA, Lodi L et al (2017) ExoMol molecular line lists XIX: high accuracy computed line lists for $H_2^{17}O$ and $H_2^{18}O$. Mon Not R Astron Soc 466:1363–1371. https://doi.org/10.1093/mnras/stw3125

33. Polyansky OL, Kyuberis AA, Zobov NF et al (2018) ExoMol molecular line lists XXX: a complete high-accuracy line list for water. Mon Not R Astron Soc 480:2597–2608. https://doi.org/10.1093/mnras/sty1877

34. Rösch F (2014) Introduction. De Gruyter Textbook, De Gruyter, https://books.google.com.br/books?id=gA_oBQAAQBAJ

35. Rothman LS, Jacquemart D, Barbe A et al (2005) The HITRAN 2004 molecular spectroscopic database. J Quant Spectrosc Radiat Transf 96:139–204. https://doi.org/10.1016/j.jqsrt.2004.10.008

36. Sahoo B, Charan N, Asutosh s, et al (2012) Inorganic Chemistry. PHI Learning, https://books.google.com.br/books?id=8KAemlQzOj8C

37. Schramm S, Schäfer M (2016) New Horizons in Fundamental Physics. FIAS Interdisciplinary Science Series. Springer, Berlin

38. Shokr M, Sinha N (2015) Sea ice: physics and remote sensing geophysical monograph series. Wiley, UK

39. Sun D (2011) Handbook of Frozen Food Processing and Packaging, 2nd edn. Taylor and Francis

40. Tennyson J, Kostin MA, Barletta P et al (2004) DVR3D: a program suite for the calculation of rotation-vibration spectra of triatomic molecules. Comput Phys Commun 163:85–116. https://doi.org/10.1016/j.cpc.2003.10.003

41. Tennyson J, Hill C, Yurchenko SN (2013) Data structures for ExoMol: Molecular line lists for exoplanet and other atmospheres. In: 6th international conference on atomic and molecular data and their applications ICAMDATA-2012, AIP Conference Proceedings, vol 1545. AIP, New York, pp 186–195, https://doi.org/10.1063/1.4815853

42. Tennyson J, Yurchenko SN, Al-Refaie AF et al (2020) The 2020 release of the ExoMol database: Molecular line lists for exoplanet and other hot atmospheres. J Quant Spectrosc Radiat Transf 255:107228. https://doi.org/10.1016/j.jqsrt.2020.107228

43. Zohar A, Snoj L (2019) On the dose fields due to activated cooling water in nuclear facilities. Progress in Nuclear Energy 117:103042. https://doi.org/10.1016/j.pnucene.2019.103042

44. Vallero D, Letcher T (2012) Unraveling Environmental Disasters. Elsevier

45. Vidler M, Tennyson J (2000) Accurate partition function and thermodynamic data for water. J Chem Phys 113:9766–9771

46. Voronin BA (2020) Method of estimation of self-broadening parameters of spectroscopic lines on the example of the $^{32}S^{16}O_2$ molecule. Optika Atmosfery i Okeana 33(11):849–853. https://doi.org/10.15372/AOO20201104

47. Voronin BA, Bykov AD (2021) Calculation of vibrational levels of H_2^XO (where X=11,…,26). Proceedings of SPIE 11916:1191605. https://doi.org/10.1117/12.2603166

48. Voronin BA, Lavrentieva NN, Mishina TP et al (2010) Estimate of the $J'J''$ dependence of water vapor line broadening parameters. J Quant Spectrosc Radiat Transf 111:2308–2314

49. Voronin BA, Tennyson J, Tolchenov RN et al (2010) A high accuracy computed line list for the HDO molecule. Mon Not R Astron Soc 402:492–496

50. Voronin BA, Tennyson J, Lodi L et al (2019) The VoTe room temperature $H_2^{16}O$ line list up to 25000 cm^{-1}. Opt Spectrosc 117:967–973. https://doi.org/10.1134/S0030400X19120397

51. Voronin BA, Makarova MV, Poberovskii AV et al (2021) The absorption spectrum of short-lived isotopic variant of water, $H_2^{15}O$: Tentative detection at the Earth's atmosphere. J Quant Spectrosc Radiat Transf 276:107929. https://doi.org/10.1016/j.jqsrt.2021.107929

52. Voronin BA, Tennyson J, Chesnokova TY et al (2024) The infrared absorption spectrum of the $H_2^{14}O$ radioactive isotopologue of water. Mol Phys 10(1080/00268976):2333474

53. Voronin BA, Tennyson J, Yurchenko SN et al (2024) The infrared absorption spectrum of radioactive water isotopologue $H_2^{15}O$. Spectra Chimica Acta A 311:124007. https://doi.org/10.1016/j.saa.2024.124007

54. Yurchenko SN, Al-Refaie AF, Tennyson J (2018) ExoCross: A general program for generating spectra from molecular line lists. Astron Astrophys 614:A131. https://doi.org/10.1051/0004-6361/201732531

55. Zohar A (2017) Snoj L (2017) Gamma Dose Field due to Activated Cooling Water in a Typical PWR. In: Cizelj L, Holler T (eds) 26TH INTERNATIONAL CONFERENCE NUCLEAR ENERGY FOR NEW EUROPE (NENE 2017), 26th International Conference Nuclear Energy for New Europe (NENE). SLOVENIA, SEP, Bled, pp 11–14